

Slow-Moving Phase Boundary in $\text{Li}_{4/3+x}\text{Ti}_{5/3}\text{O}_4$

Yug Joshi,* Robert Lawitzki, and Guido Schmitz

Lithium titanate is one of the most promising anode materials for high-power demands but such applications desire a complete understanding of the kinetics of lithium transport. The poor diffusivity of lithium in the completely lithiated and delithiated (pseudo spinel) phases challenges to explain the high-rate performance. This study aims at clearing the kinetics of lithium transport using an innovative technique that employs optical microscopy in a constrained region of sputter-deposited thin-film samples. It enables the in situ observation of the transport of lithium through the electrode. Furthermore, with a thermostatically controlled cell, the Arrhenius-like temperature dependence is revealed. The quantitative findings demonstrate that indeed the end phases have poor diffusivity which is, however, accelerated at intermediate Li concentrations in the spinel structured $\text{Li}_{4/3+\delta}\text{Ti}_{5/3}\text{O}_4$ phase. Surprisingly, the slow migration of the phase boundary hinders the formation of the Li-rich (rock-salt) phase in the initial stages. Such kinetic control by the phase boundary stands in obvious contrast to a prior (theoretical) study postulating almost “liquid” behavior of the interface. Only after the Li diffusion into the Li-poor (spinel) phase has faded, when approaching the solubility limit, the further growth of the rock-salt phase becomes diffusion controlled.

the material was first explored by Murphy et al. in 1983,^[3] but only in 1995 Ohzuku et al. demonstrated its use in lithium-ion battery application and reported a nearly constant dis-/charge voltage of 1.55 V versus Li/Li^+ .^[4] The constant voltage for de-/intercalation is indicative of a phase transformation during lithium insertion/removal. However, the existence of a two-phase reaction at room temperature and on a macroscopic scale has been debated in the past, with reports suggesting solid-solution^[5] and/or nano-domains^[6] in an equilibrium condition. Nevertheless, the existence of the two phases was confirmed by direct imaging individual phases using high-resolution transmission electron microscopy (TEM).^[7]

A cubic unit-cell of $\text{Li}_{4/3}\text{Ti}_{5/3}\text{O}_4$ has 8 formula units with 32 oxygen atoms located at the 32e sites, 1/3rd of the lithium and all of the titanium atoms are occupying 16d sites (octahedral positions) and the remaining 8 atoms of lithium are at 8a


sites (tetrahedral positions).^[8] During the phase transformation to $\text{Li}_{7/3}\text{Ti}_{5/3}\text{O}_4$ upon lithium insertion, the atoms of lithium at the 8a sites shift to the neighboring 16c position (octahedral position) and the insertion of eight additional lithium atoms takes place in the remaining 16c positions thus filling up all of the octahedral sites.^[4,8] This reordering and insertion of lithium atoms, is accompanied by a huge change in the electronic^[8] and the optical properties.^[9] However, structurally, there is a mere 0.2% change in the volume of the unit-cell (hence the term “zero-strain” phase transformation was coined).^[4]

The fast dis-/charge ability of LTO (practically achieved by surface modification and reducing particle size)^[2] must be governed by the transport properties of lithium and the kinetics of phase propagation in the electrode, provided, the electronic conductivity is sufficient. Ganapathy et al.,^[16] using first-principle calculations, addressed the migration across the phase boundary and its movement during the phase transformation to explain the fast dis-/charging ability of this material. Their calculation suggests that a fast migration in and out of the phase boundary enables the phase boundary to move almost like a “liquid.” This would be in contrast to some silicon-based^[10–12] and hydrogen-based systems^[13,14] where the interface between structurally different phases is known to hinder the migration of atoms. Such hindrance at the phase boundary would lead to a deviation from a normal diffusion-controlled parabolic growth to a slower interface-controlled linear growth of the silicide or hydride phase in the initial stages of atomic transport. This study is aimed at experimentally determining the migration of

1. Introduction

The need for fast dis-/charging batteries to power electric or hybrid vehicles is at an all-time high and will only increase, at least in the near future. Li-ion battery technology is the current state-of-the-art of electrochemical energy storage. Furthermore, lithium titanate or $\text{Li}_{4/3}\text{Ti}_{5/3}\text{O}_4$ (LTO) is considered as one of the most promising anode materials for high power applications, owing to its safe operating voltage, high cyclic stability, and “zero-strain” phase transformation during de-/intercalation of lithium (i.e., $\text{Li}_{4/3+\delta}\text{Ti}_{5/3}\text{O}_4$ or Li-poor ‘spinel’ phase being transformed into $\text{Li}_{7/3-\delta}\text{Ti}_{5/3}\text{O}_4$ or Li-rich ‘rock salt’ phase upon lithium insertion).^[1,2] The possibility of lithium insertion in

Y. Joshi, R. Lawitzki, G. Schmitz
Chair of Materials Physics
Institute of Materials Science
University of Stuttgart
70569 Stuttgart, Germany
E-mail: yug.joshi@mp.imw.uni-stuttgart.de

 The ORCID identification number(s) for the author(s) of this article can be found under <https://doi.org/10.1002/smt.202100532>.

© 2021 The Authors. Small Methods published by Wiley-VCH GmbH. This is an open access article under the terms of the Creative Commons Attribution-NonCommercial License, which permits use, distribution and reproduction in any medium, provided the original work is properly cited and is not used for commercial purposes.

DOI: 10.1002/smt.202100532

the phase boundary caused by the insertion of lithium. To our knowledge, the possible existence and kinetics effects, if any, of such a barrier at the phase boundary between Li-poor and Li-rich titanate have not yet been discussed or even experimentally explored. Presumably, this is due to the conventional assumption of a diffusion-controlled parabolic growth.

Essentially, in a battery material, the diffusion proceeds through the bulk of the material, but the methods with which such migration can be studied in-operando are limited. It is achieved here by using an innovative and effective technique that exploits the change in the optical properties of LTO upon lithium insertion, that is, the electrochromic (EC) character of LTO, especially in the red wavelength region of the visible spectrum which has been characterized and quantitatively modeled in a recent publication.^[9] The method incorporates obstructing a small area of a dense thin-film electrode by an optically transparent Li-ion blocking layer (Kayaku Advanced Materials SU-8 photo/e-beam resist coated using e-beam lithography). Subsequently, lithium is electrochemically inserted through the uncovered area. This allows for monitoring the optical change (with the help of an optical microscope) caused by the transport of lithium underneath the transparent blocking layer (i.e., through the bulk of the electrode material). The methodology enables us to “literally” observe the propagating $\text{Li}_{7/3}\text{Ti}_{5/3}\text{O}_4$ phase-front in the electrode. The thin-film geometry and the experimental setup are shown in **Figure 1a** and **b**, respectively. The sample preparation and details of the setup are described in the Experimental Section. The migration of Li underneath the SU-8 is used to visualize the volume transport, however, only in an ideal 1D and/or 2D diffusion geometry. But, since LTO has a cubic symmetry in both phases, diffusion must be isotropic. This holds even more for a nano-crystalline microstructure with random orientation of the grains. Thus, the transport coefficients and the migration of the phase boundary evaluated here in 1D or 2D diffusion couples represent nevertheless the generic transport properties of the material. The micrometer range of the investigated diffusion length makes the results relevant for a commercial battery application (dealing with particles of sizes close to a few micrometers or less).

It should be pointed out that both the rock-salt and the spinel phases have the same spatial arrangement of Ti and oxygen atoms with only a negligible change in the lattice parameter upon

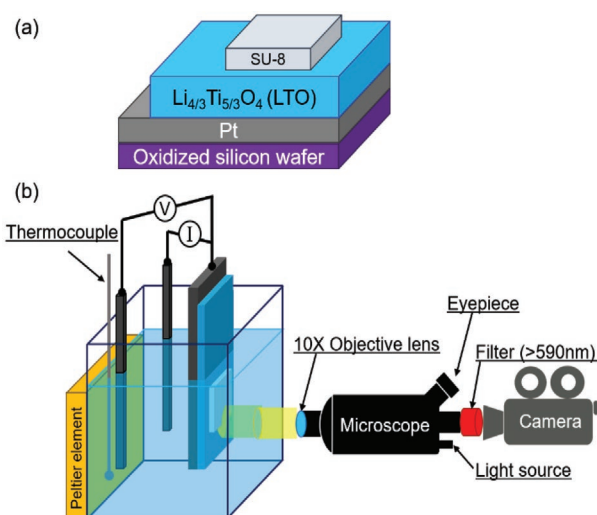


Figure 1. a) Schematic of the electrode sample coated with e-beam resist SU-8. b) Setup for electrochromic imaging with simultaneous electrochemical intercalation/deintercalation of lithium ions in a three-electrode battery setup.

lithium insertion (8.3562 Å for spinel and 8.3523 Å for rock-salt phase).^[15] Hence, any kind of structural characterization, to differentiate between the phases, by diffraction techniques is highly ambiguous. The non-resolvability of the individual phases using X-ray diffraction and selected area electron diffraction (SAED) has already been reported.^[15,16] This makes the herein described methodology particularly attractive also for characterizing other battery materials with insignificant change in lattice parameter upon intercalation but showing EC behavior.^[17–21]

2. Results

2.1. Structure and Morphology

Figure 2 shows the structure and morphology of the LTO electrode and the coated SU-8 e-beam resist. **Figure 2a** shows the scanning electron microscope (SEM) image of a corner of the coated SU-8 barrier on top of the LTO electrode. A sharp

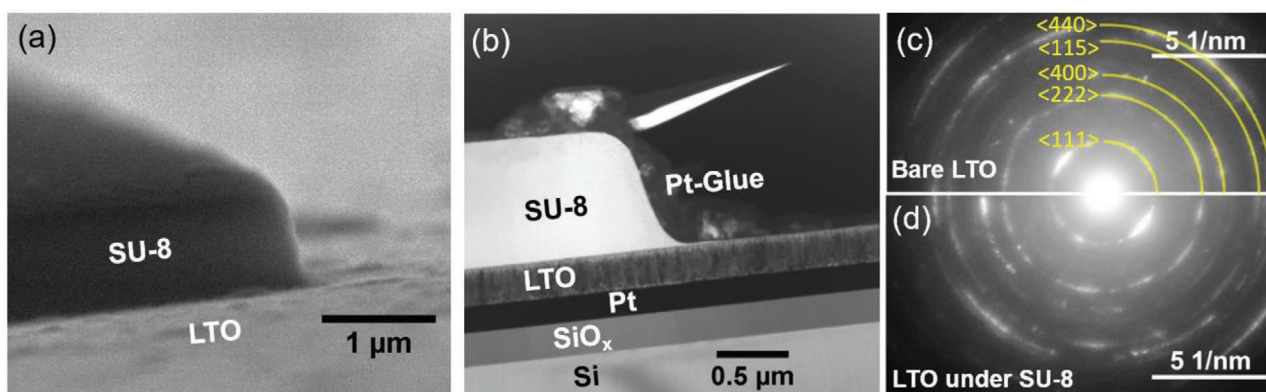


Figure 2. a) SEM image of SU-8 film coated on LTO electrode; b) TEM image of the multilayer stack with the SU-8 coating; c) diffraction pattern of the LTO layer without the SU-8 coating; d) LTO layer underneath the SU-8 coating.

interface between the SU-8 and LTO can be observed. For a closer look at the coated barrier layer and the sputtered LTO thin-film, a cross-section of the multilayered sample is analyzed using bright-field TEM in Figure 2b. The thickness of the SU-8 layer and the width of the edge are ≈ 860 and ≈ 350 nm, respectively. Thus the edge is definitely sharper than the optical resolution of the $10\times$ objective lens used in the experimental setup (with a resolving power of $1\ \mu\text{m}$). From Figure 2b a columnar grain morphology is confirmed in the LTO layer of ≈ 250 nm in thickness, as formed in the sputter deposition growth process. Figure 2c,d shows the SAED patterns from the LTO layer, away and underneath the SU-8 coating, respectively. The diffraction patterns confirm the desired spinel structure. Furthermore, there is no change in the crystal structure of the LTO electrode, hence it can be concluded that the lithography process does not alter the crystal structure of the LTO electrode used for the kinetic studies.

2.2. Migration of Lithium

As mentioned before, the fast dis-/charging ability of the LTO (also confirmed for the herein used thin-films in Figure S1, Supporting Information) must relate to fast transport of lithium.^[2] Therefore, this transport is probed via electrochromic imaging (see the Experimental Methods). **Figure 3** shows the migration of lithium at room temperature, $22\ ^\circ\text{C}$. As seen in Figure 3a, the intercalation process is initiated at time $t = 0$ s by applying a voltage step (black line) from 2.72 V (the open-circuit voltage, OCV of the electrode) to 1 V versus Li/Li^+ . This application of a step voltage to 1 V initiates an extremely fast charging process in the uncoated film areas. The respective current response is shown by the red dotted line. The schematic in the inset of Figure 3a indicates the area recorded by the optical microscope, a yellow circle where the light from the $10\times$ objective lens is incident. A top view of the LTO electrode coated with the SU-8 barrier, as recorded by the optical microscope, is shown in Figure 3b. The image was taken just before the voltage step was commenced (at $t = 0$ s). Due to the transparent nature of the SU-8, there is no observable difference in the intensity between the coated and uncoated LTO. The interface/edge between the uncoated LTO and the blocked LTO layer is visible as a dark line caused by local scattering. The position of this edge has been highlighted by a white dashed-dotted line in Figures 3c–g. Figure 3c shows the image taken 120 s after applying the voltage step. The uncoated part of the LTO has completely turned black by absorption of all the incident red-light. This is due to the phase transformation to completely lithiated $\text{Li}_{7/3}\text{Ti}_{5/3}\text{O}_4$ which is known to significantly absorb the red light.^[9] As intended, the blocked part has not transformed at all. Only after 9000 s (see Figure 3d), a darker gray band has formed ahead of the edge/interface (between the blocked LTO layer and bare LTO), suggesting bulk migration of lithium into the LTO layer underneath the SU-8. At time $t = 30\ 120$ s (Figure 3e), this gray band has progressed even further. In Figure 3f at time $t = 150\ 960$ s, appearance of a new fully black stripe becomes noticeable, indicating the progress of a second phase. This “black” phase has even grown further as time progresses to

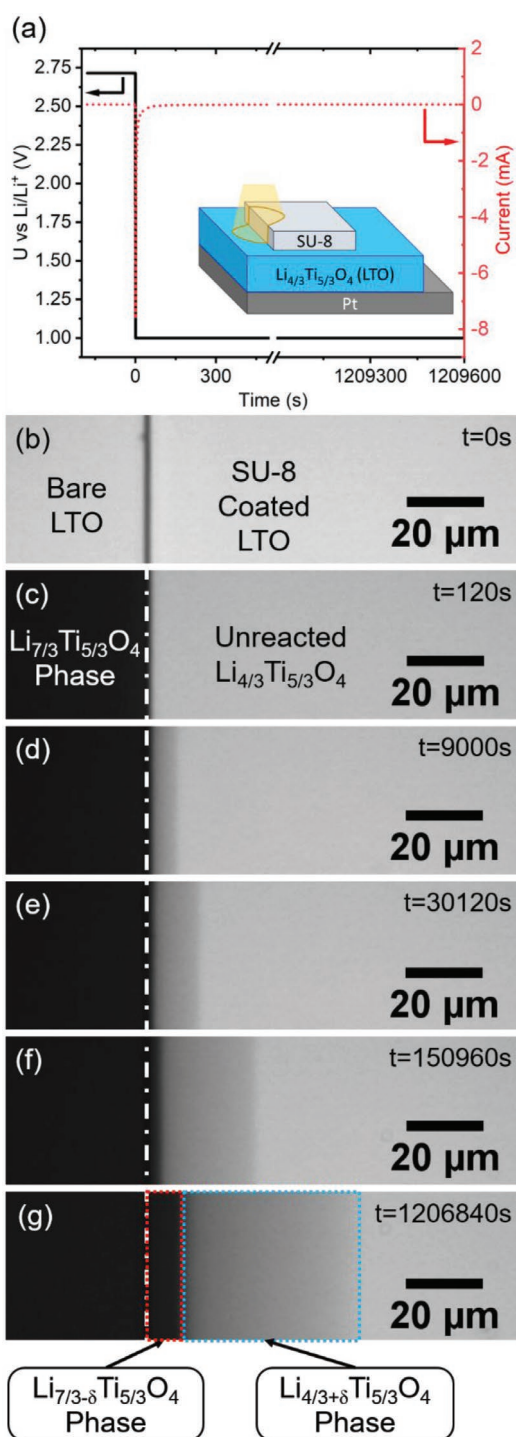


Figure 3. a) A constant voltage of 1 V is applied at 0 s and is maintained throughout the experiment; inset schematic clarifies the field of view from the microscope (yellow). From (b) to (g), gray scale images showing the lithium diffusion into the LTO underneath the barrier layer, at different times, b) $t = 0$; c) $t = 120$ s; d) $t = 9000$ s; e) $t = 30\ 120$ s; f) $t = 150\ 960$ s; g) $t = 1\ 206\ 840$ s. The white dot-dashed line represents the interface between the bare LTO (left) and the LTO covered with SU-8 (right). In (g), the region of the Li rich $\text{Li}_{7/3-\delta}\text{Ti}_{5/3}\text{O}_4$ phase is highlighted by a red rectangle, the region of the weakly lithiated phase $\text{Li}_{4/3+\delta}\text{Ti}_{5/3}\text{O}_4$ by a blue rectangle. (δ represents a small change in concentration.) Remaining light grey at the right hand side represents still completely delithiated $\text{Li}_{4/3}\text{Ti}_{5/3}\text{O}_4$ phase.

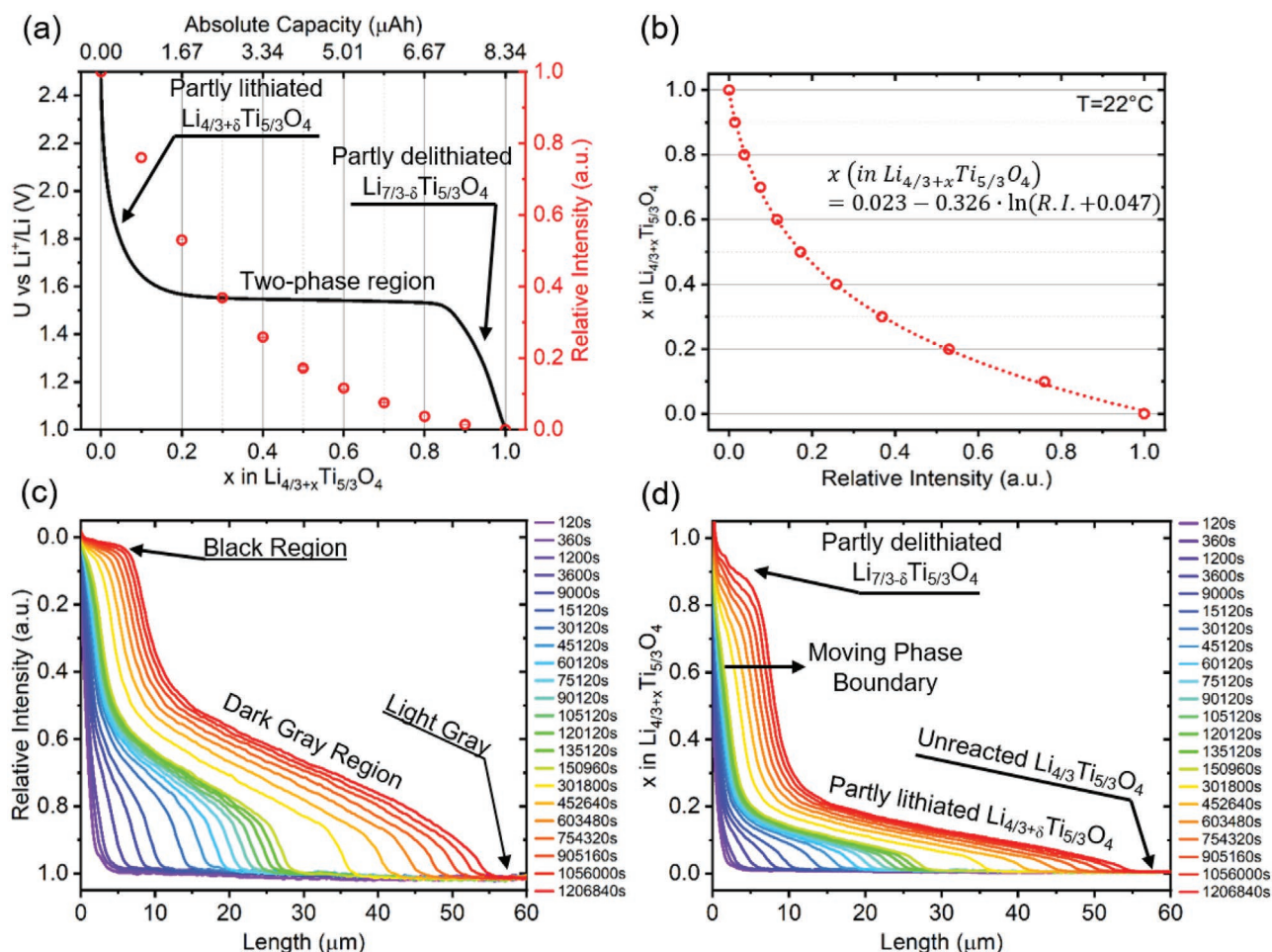


Figure 4. a) Evolution of voltage profile as a function of lithium concentration (black solid) and the corresponding relative intensity (red circles); b) relative intensity versus Lithium concentration obtained experimentally as shown by hollow red circles and a corresponding fitted curve shown by the red dashed curve. The curve represents a logarithmic decay curve with the equation given in the legend. c) Relative Intensity profile at different times; d) Concentration profiles derived from the relative intensity profiles, with the help of the curve as shown in (b).

$t = 1\,206\,840$ s (13 days, 23 h, and 14 min) in Figure 3g. The measurement was stopped after 2 weeks.

To evaluate the above-obtained images in terms of lithium concentration and phase evaluation, a calibration measurement was executed as shown in Figure 4. For this, a similar sample was intercalated galvanostatically at a C rate of ≈ 0.1 C (i.e., a single charging or discharging step takes roughly 10 h). The corresponding voltage profile of the LTO electrode is shown in Figure 4a (black solid) which clearly reflects a two phases equilibrium by the constant voltage (chemical potential of Li) at intermediate average Li concentration. Simultaneously, the intensities were recorded at regular intervals from the area not covered by SU-8 (see also supplementary data Figure S3, Supporting Information). These are then converted into relative intensity by assuming the intensity of light reflected from the pure $\text{Li}_{4/3}\text{Ti}_{5/3}\text{O}_4$ phase is 1 and that from the fully lithiated $\text{Li}_{7/3}\text{Ti}_{5/3}\text{O}_4$ phase is 0. Accordingly, at different charge states, the relative intensities are obtained as shown by red hollow points in Figure 4a. The apparent continuous transition of the intensity in the two-phase region is due to the stacking of both the phases in the viewing direction. Combining the data

on intercalation and intensity, a calibration curve is obtained as depicted in Figure 4b. The equation of the curve is noted in the figure. Utilizing this calibration curve the relative intensity profiles, obtained during the diffusion experiment as shown in Figure 4c, are converted to the concentration profiles in Figure 4d.

The steep jump of lithium concentration between $x = 0.85$ to $x = 0.2$ (where x is the amount of lithium in $\text{Li}_{4/3+x}\text{Ti}_{5/3}\text{O}_4$) clearly indicates a phase boundary, best visible for the longest time step (i.e., 1 206 840 s). Now, correlating Figure 3g with Figure 4d, the concentration in the different gray-scale regions can be identified. In Figure 3g, moving from left to right, the black region prior to the coating edge is the fully intercalated rock salt (or Li-rich phase). The black stripe directly to the right of the edge represents a partially delithiated rock salt phase. To the right of this black stripe, the darker gray band belongs to the partially lithiated spinel (or Li-poor phase), and finally, the unmodified light gray to the far-right side represents the unreacted pure LTO or 'pseudo spinel'. A detailed point to note, in the concentration profiles of Figure 4d, at the position of $0 \mu\text{m}$, the concentration even increases beyond the theoretical

maximum of $x = 1$. This is an artifact owing to the additional scattering by the edge of the SU-8 coating. Similar concentration profiles, only with faster kinetics, were obtained at higher temperatures of 45 and 55 °C and are shown in the supplementary data.

For diffusional transport with a constant diffusion coefficient, the concentration profile of the diffusor should match an error function (for semi-infinite diffusion from a constant source). In contrast, the concentration profile of the spinel region falls quite abruptly to the completely unreacted pseudo spinel, indicating a huge variation of the diffusion coefficient in this concentration range. This agrees well with the literature^[6,22–27] reporting a very slow diffusion in pseudo spinel that increases steeply with a small increase of lithium content. In a steady-state evolution of the concentration profile, a low diffusion coefficient has to be compensated by a stronger concentration gradient which provokes a pronounced contrast between the initial fully delithiated (pseudo spinel) and the partially lithiated spinel phase, although thermodynamically, both belong to the same phase.

Since the optical resolution of the microscopy is less than the lateral grain size, the continuous gray-shading in Figure 3d to (g) has to be interpreted by the Harrison's type A diffusion,^[28] that is, bulk and grain boundary diffusion cannot be distinguished and so the measured diffusion coefficient may have a contribution from fast grain boundary transport. However, since generally used LTO particles in commercial batteries also constitute many grains and grain boundaries,^[27,29–31] the so obtained transport coefficients (having contribution from GB's) are indeed the practically relevant ones. The discontinuous jump in the concentration profile between the black stripe and the dark grey region confirms a two-phase reaction on a macroscopic scale. A continuous solid solution or formation of nano-domains of the two phases as frequently claimed^[5,6] is evidently inconsistent with these experimental observations.

2.3. Growth Kinetics of the Rock Salt Phase: A Linear to Parabolic Transition

The concentration profiles at different time intervals enable an accurate characterization of the kinetics of lithium migration and the phase transformation in the LTO electrode, measured by the width of the formed phases. Reactive diffusion has been intensively investigated in the case of the interdiffusion of metallic diffusion couples.^[32] In the case of a steady-state transport, parabolic growth (i.e., thickness proportional to the square root of time) of intermetallic reaction products is a common observation.^[33,34] In the very early stages, however, a deviation toward linear growth (thickness proportional to time) is expected, although rarely experimentally proven in the reaction of metals. The respective kinetic coefficient for the linear growth, in particular, its temperature dependence and activation energy are widely unexplored. Extended linear regimes might be seen, if the reaction at the phase boundary requires a major reordering of the atomic arrangement at an interface particularly in the context to fast interstitial diffusion, for instance, with the growth of silicides^[10–12] and hydrides.^[13,14] Such interface-controlled transport results in a slow linear growth of the intermetallic/hydride phase in the initial stages of atomic transport (see ref. ^[35]) rather than a faster parabolic growth.^[10,12] To

allow for such linear growth, we describe the temporal evolution of the width of the Li-rich rock salt phase by Equation (1):

$$t = \frac{c^R - c_{\max}^S}{\kappa \cdot (c^R - c_{\min}^R)} (w - w_0) + \frac{c_{\min}^R - c_{\max}^S}{2D_{Li}^R \cdot (c^R - c_{\min}^R)} (w^2 - w_0^2) \quad (1)$$

which is inspired by the work of Gösele and Tu,^[36] and Tomán et al.^[35] and further derived in the supplementary information. The variable t denotes the time, c^R is the maximum concentration (atomic fraction of Li on the octahedral sites) of the rock salt phase which equals 1. c_{\min}^R and c_{\max}^S are the concentrations of both sides of the phase boundary, that is, on the Li-rich side $c_{\min}^R = 0.85$ and on the Li-poor side $c_{\max}^S = 0.15$ (from Figure 4a). κ is the “barrier” coefficient controlling the linear growth, w is the width of the phase, w_0 is a possible initial width (in our case, very close to zero) and D_{Li}^R is the chemical diffusion coefficient of Li in the rock salt phase (in principle concentration-dependent but here averaged over the composition range of the phase in the sense of a Wagner integral^[37]).

For quantification, we define the position of the interface between the two phases at the concentration $x = 0.7$ in $\text{Li}_{4/3+x}\text{Ti}_{5/3}\text{O}_4$ as this concentration clearly falls into the two-phase region. Figure 5a shows the evaluated widths of the Li-rich phase as a function of time at different temperatures. Consider the room temperature measurement (22 °C, gray squares). It is evident that the rock salt phase starts to grow first proportional to time as marked by a gray dotted line with a slope of $m_l = 6.77 \times 10^{-10} \text{ cm} \cdot \text{s}^{-1}$. Only at a later time, it deviates from this linear growth and finally reaches the parabolic regime, as clearly demonstrated by a plot of the square of the width versus time (see Figure 5b), in which the late data points agree to a straight line with slope $m_p = 5.32 \times 10^{-13} \text{ cm}^2 \cdot \text{s}^{-1}$. By using these measured slopes and Equation (1), we determine the effective diffusion coefficient and the barrier coefficient. Also, from the ratio between both, we determine the critical thickness of the rock salt phase at which linear and parabolic growth rates become identical ($w_{cr}^R = \frac{m_p}{m_l} / 2$). It marks the thick-

ness that the Li-rich phase has to reach so that further growth becomes diffusion-limited. The barrier coefficient κ at room temperature amounts to $3.84 \times 10^{-9} \text{ cm} \cdot \text{s}^{-1}$ while the diffusion coefficient of Li in the rock salt phase is determined to $1.24 \times 10^{-12} \text{ cm}^2 \cdot \text{s}^{-1}$. Similar observations are made at other temperatures (see Figures 5a,b). The respective transport coefficients along with the respective critical thicknesses w_{cr}^R , the time to reach this thickness t_{cr} (calculated using Equation (1)) are listed in Table 1.

It should be pointed out that the derivation of Equation (1) assumes all the incoming flux is used to grow the Li-rich rock salt phase. This is not completely true, as the spinel phase is simultaneously consuming lithium from the incoming flux, as can be seen in Figures 3 and 4d. Nevertheless, Equation (1) provides an efficient method to describe the linear to parabolic transition and to quantify the barrier coefficient. But strictly, a correct evaluation of the diffusion coefficients has to use the Boltzmann–Matano (BM) method for semi-infinite geometry in the parabolic regime.^[32,38–41]

This method considers the full concentration profile at a selected time within the parabolic regime. With this, the

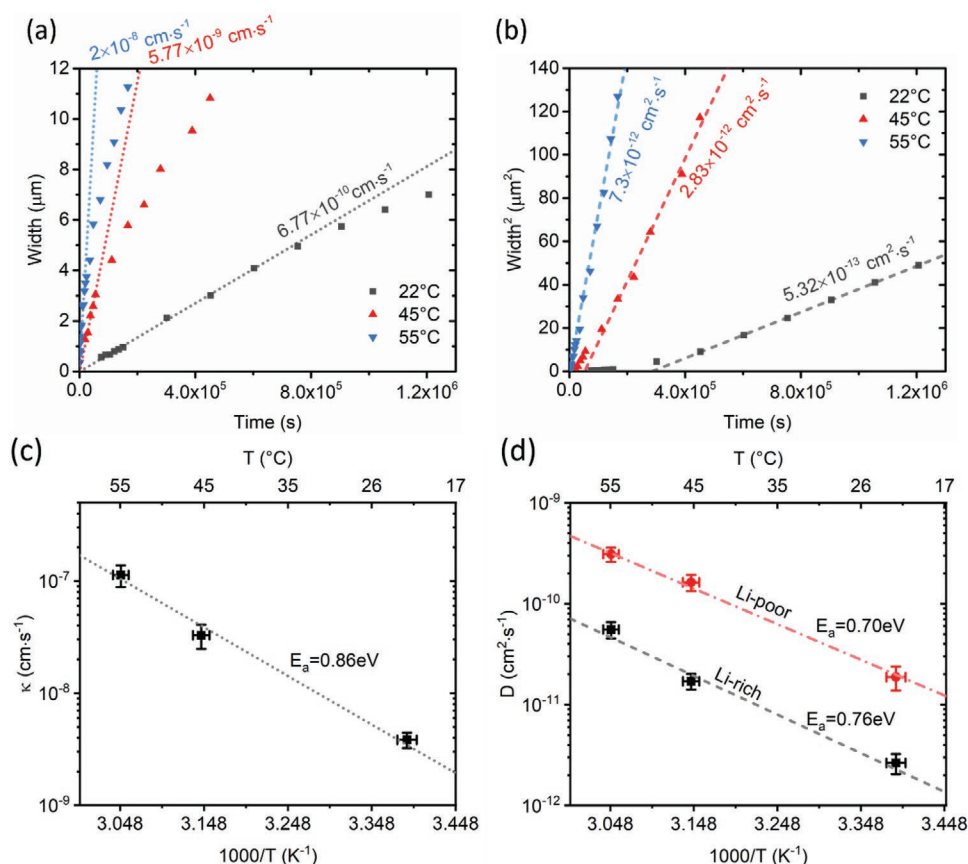


Figure 5. Kinetics of the shift of the phase boundary between the lithium rich phase ($\text{Li}_{7/3-\delta}\text{Ti}_{5/3}\text{O}_4$) and lithium poor phase ($(\text{Li}_{4/3+\delta}\text{Ti}_{5/3}\text{O}_4)$) at 22, 45, and 55 °C. a) Width of lithium rich phase versus time; b) Square of width of lithium rich phase versus time. Temperature dependence of c) the linear growth constant κ and d) the parabolic growth constant D .

diffusion coefficient is evaluated for any given c^* along the concentration profile as:

$$D(c^*) = -\frac{1}{2t} \frac{dx}{dc} \Big|_{c^*} \int_0^{c^*} (x - x_M) dc \quad (2)$$

As usual, t is the time during which the composition profile has developed by diffusion, dx/dc represents the reciprocal of the concentration gradient at the selected position c^* , and $(x - x_M)$ is the distance from a reference plane situated at x_M . In the present case, x_M has to be set to 0 (edge of the protective coating), as at this plane the concentration remains fixed.^[39,40] Practically, the integral represents the area under the concentration profile taken along the concentration axis or y -axis in

Figure 4d. This area is bounded by the concentration at which the diffusivity is evaluated and by the lowest concentration of mobile lithium (i.e., between $x = c$ and $x = 0$ in $\text{Li}_{4/3+x}\text{Ti}_{5/3}\text{O}_4$). Using Equation (2), the diffusion coefficients at concentrations $c = 0.88$ (for the rock salt phase) and $c = 0.1$ (for the spinel phase) have been evaluated. These corrected diffusivities are also given in Table 1 (from Equation (2)). It is sufficiently clear that in comparison diffusivities evaluated earlier with Equation (1) are slightly underestimated. Based on the determined diffusivity, we also have evaluated for later discussion the diffusion depth in the spinel phase at the critical transition time ($w_{cr}^s = \sqrt{D_{Li}^s \cdot t_{cr}}$).

The diffusion coefficient for the Li-poor spinel phase is evaluated to be $1.88 \times 10^{-11} \text{ cm}^2 \cdot \text{s}^{-1}$ and that of the Li-rich rock salt phase to $2.65 \times 10^{-12} \text{ cm}^2 \cdot \text{s}^{-1}$ at room temperature. This

Table 1. Diffusion coefficients of Li in the Li-rich rock salt phase, barrier coefficient and its corresponding critical thicknesses of the rock salt phase at different temperatures, critical time to reach this thickness, diffusion coefficient of Li in the α phase, and the corresponding width of the spinel phase at the critical time.

Temp [°C]	D_{Li}^R [$\times 10^{-12} \text{ cm}^2 \cdot \text{s}^{-1}$] From Equation (1)	D_{Li}^R [$\times 10^{-12} \text{ cm}^2 \cdot \text{s}^{-1}$] From Equation (2)	κ ($\times 10^{-9} \text{ cm} \cdot \text{s}^{-1}$) From Equation (1)	w_{cr}^R [μm]	t_{cr} [$\times 10^3 \text{ s}$]	D_{Li}^S [$\times 10^{-11} \text{ cm}^2 \cdot \text{s}^{-1}$] From Equation (2)	w_{cr}^S [μm]
22 °C	1.24 ± 0.2	2.65 ± 0.6	3.84 ± 0.6	3.93	870.8	1.88 ± 0.5	40.4
45 °C	6.60 ± 1.5	17.1 ± 3	32.7 ± 8	2.45	63.7	16.3 ± 3	32.5
55 °C	17.0 ± 2	55.4 ± 10	113 ± 25	1.8	13.7	31 ± 5	20

signifies that the diffusion in the Li-poor phase is roughly seven times that of the Li-rich phase. Based on electrochemical impedance spectroscopy, Wang et al.^[27] reported the Li diffusivity in the spinel and rock salt phase equals $2.2 \times 10^{-11} \text{ cm}^2 \cdot \text{s}^{-1}$ and $3 \times 10^{-12} \text{ cm}^2 \cdot \text{s}^{-1}$, respectively, which is in convincing agreement with the values determined here. Increased diffusivities in the Li-poor phase were also observed by Schmidt et al.^[22] using NMR. From their reported activation energy and pre-factor, at 22 °C, the spinel is predicted to show a diffusion coefficient of $1.74 \times 10^{-12} \text{ cm}^2 \cdot \text{s}^{-1}$ whereas the rock salt has a diffusivity of only $1.19 \times 10^{-13} \text{ cm}^2 \cdot \text{s}^{-1}$.^[22] Reproducing the relative trend between both phases, the absolute values determined from NMR are nevertheless an order of magnitude lower. Since both studies concern nanocrystalline materials, this discrepancy is probably because the diffusivities determined from NMR are representative of self-diffusion whereas the values determined here represent chemical diffusion coefficients (including the thermodynamic factor). The thermodynamic factor ($\Phi = c \cdot (1 - c) / (k_B T) \cdot \partial \mu / \partial c$; where c is equivalent to x in $\text{Li}_{4/3+x}\text{Ti}_{5/3}\text{O}_4$ and the derivative of the chemical potential is determined from the CP measurement) for the rock salt and spinel phases ($x = 0.88$ and $x = 0.1$ in $\text{Li}_{4/3+x}\text{Ti}_{5/3}\text{O}_4$) are roughly 9 and 5.7. Therefore, when the thermodynamic factor is considered, the herein reported values of the diffusion coefficient are also in close agreement to the ones determined from NMR measurements of the jumping rate that represent tracer diffusivities.

The here confirmed significant difference in the diffusivities of the rock salt and the spinel phases may be heuristically understood from the different interstitial arrangement of both phases. While in the slightly lithiated spinel, Li occupies both sites (8a and 16c), but still ample of vacant 16c sites are available, in the slightly delithiated rock salt, exclusively 16c sites are occupied. Successful elementary diffusion steps need, however, consecutive jumps in the sequences c-a-c or a-c-a, which are obviously more difficult to be realized in the rocksalt phase where the jump to an 8a site forms an energy demanding defect while vice versa, jumps to occupy a 16c sites belong to the equilibrium of the spinel phase.

Now, from the transport coefficients at different temperatures (see Table 1) the determination of the activation energies is made possible. Respective Arrhenius plots are presented in Figure 5c,d. The values for the diffusivities are the ones determined from the BM method. The data of both transport coefficients agree quite well with Arrhenius-like dependences. Although the range of temperature variation is still quite low (limited by the stability of the liquid electrolyte, see Experimental methods) the precision of the individual data points and the low reference temperature (295 K) may still justify the statement of meaningful activation energies. The activation energy for the barrier coefficient is $0.86 \pm 0.05 \text{ eV}$, whereas for the two diffusion coefficients they are $0.70 \pm 0.05 \text{ eV}$ and $0.76 \pm 0.05 \text{ eV}$ in the spinel and rock salt phase, respectively. The higher activation energy of the barrier coefficient signifies a stronger temperature dependence and so, at low temperatures, the phase propagation is controlled by the slowly migrating interface for a considerable duration.

The activation energy of the chemical diffusion coefficient evaluated here can be compared with other reports. Wilkening et al.^[42] stated an activation energy of 0.86 and/or 0.94 eV for

the completely delithiated LTO using spin-alignment echo NMR (which is sensitive to slow diffusion process) and dc-conductivity measurements, respectively. A very similar value of 0.96 eV was reported by Haetge et al.^[43] using complex impedance measurement. By contrast Schmidt et al.^[22] and Hain et al.^[23] using NMR reported a value of 0.38 and 0.39 eV for the partially lithiated spinel phase; and 0.51 and 0.45 eV for the rock salt phase. Furthermore, Ziebarth et al.,^[44] using first-principle calculations at zero K, predicted the energetic barrier for lithium migration in the Li-rich phase (16c to 8a to 16c) to be between 0.2 and 0.51 eV. However, migration from a 16d site to a 16c site required much higher activation energy ranging between 0.80 and 0.94 eV, whereas the reverse path needed an activation energy between 0.56 and 0.63 eV. In the case of Li-poor phase, Ziebarth et al. determined an activation energy of 0.48 eV for 8a-16c-8a pathway, but, for the jump from 16d to 8a a high activation energy of 0.92 eV was calculated. Chen et al.^[26] using similar ab-initio methods calculated a much higher activation energy of 0.7 eV in the Li-poor phase for the 8a-16c-8a pathway and 1 eV for the 16c-48f-16c pathway. Similarly, for the Li-rich phase they calculated an activation energy of 0.35 for a 8a to 16c jump (which represents the easy part of the full jumping sequence). Obviously, the values determined here (corresponding to 0.70 and 0.76 eV for the spinel and rock salt phase, respectively) represent an average of different jumping processes. In view of scatter between previous reports, they appear not unlikely.

2.4. Effect of Electrode Geometry

The clearly demonstrated existence of a kinetic barrier for the migration of the phase boundary prompts the question of its impact on the performance in technical battery electrodes. Generally, a battery electrode particle may be better assumed to be of finite size with an approximately spherical geometry in which 3D atomic migration is taking place toward the center. Due to the small depth of focus of the optical microscope, a 3D geometry is difficult to analyze with the present setup. But a planar cylindrical disk (representing a model geometry for 2D migration of atoms) poses no complication. Therefore, the SU-8 was coated in circular-disk geometries with varying radius, that is, $R = 2.5, 5, 10, 20 \mu\text{m}$, as shown in Figure 6a. Point to note, out of these, the 2.5 and 5 μm are close to the critical transition width determined for the rock salt phase at room temperature. Thus, we would expect that the lithiation of these smaller “particles” should be significantly slowed down by linear kinetics. The figure shows the various patterns (with varying radii on a single substrate) at $t = 0\text{s}$. Again, for electrochromic imaging of the intercalation at room temperature, the voltage step is initiated at $t = 0\text{s}$. As before, the uncovered area is transformed into the $\text{Li}_{7/3}\text{Ti}_{5/3}\text{O}_4$ phase almost immediately, as shown in Figure 6b after 120s, whereas it takes 2820s (Figure 6c) to completely transform the blocked area of 2.5 μm radius to the rock salt phase. Still, this would correspond to a charging rate faster than 1C for a relatively big particle of 5 μm in diameter (in the case of a spherical particle of the same diameter, it would be even somewhat faster due to 3D transport). Subsequently, to completely transform the areas of 5, 10, and 20 μm radius into

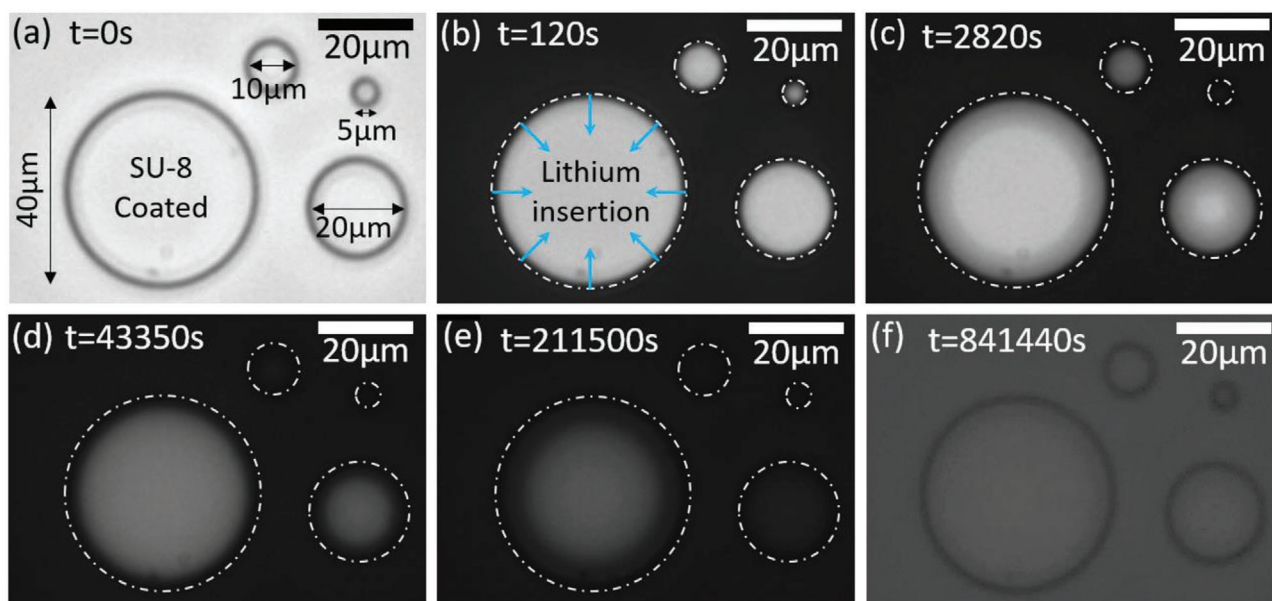


Figure 6. a) Different circular lithography patterns observed at $t = 0$ s during the electrochromic imaging experiments. b) At 120 s, all the uncovered area has transformed into the Li-rich phase (black), while the resist-coated circular areas are clearly visible. Further images taken after longer times: c) 2820 s; d) 43 350 s; e) 211 500 s and f) 841 440 s, when the patterns with radius 2.5, 5, 10, and 20 μm were completely saturated with the Li-rich phase, respectively. The contrast of (f) has been enhanced significantly to visualize the completely transformed circular patterns. In the same contrast as the other partial figures, (f) would appear completely black.

the rock salt phase, it needed 43.4, 212, and 841 ks, respectively, as shown in the corresponding Figures 6d–f. In the larger disks (10 and 20 μm radius), the migration of the phase boundary can be evaluated in detail. This confirms the existence of linear growth of the rock salt phase in the initial stages of lithiation, see Figure 7a and b, respectively. Only at a later time, diffusion-controlled growth of the rock salt phase is observed as depicted in Figure 7c,d. It comes as a surprise, however, that the critical thicknesses of the transition into the parabolic regime are systematically smaller for the circular discs in comparison to the 1D semi-infinite geometry. The critical transition thicknesses for the circular disk with 10 and 20 μm radius are 1.2 and 2.9 μm , respectively, while for the semi-infinite case discussed before, it has been 3.9 μm . It appears that the critical thickness decreases when shrinking the particle size, or in other words with decreasing available space for lithium migration. A point to note, since the critical thicknesses are reduced in the circular geometry, it takes merely 1/11th and 1/7th of the total time for lithiation in 10 and 20 μm disks, respectively, to reach the diffusion-controlled regime. Thus the lithiation is effectively controlled by parabolic growth (cf. Figures 5a, 7a,b) opposed to our initial expectation from the semi-infinite geometry.

3. Discussion

Obviously, a kinetic barrier against growth of a layer like product phase, could principally be due to two credible interfaces, first that at the phase boundary between the rock salt and spinel phases and second, the Butler–Volmer type interface at the solid/liquid interface. However, the particular geometry of our set-up excludes any significant impact of the latter, due to

the much larger contact area to the electrolyte in comparison to the transport cross-sectional area perpendicular to the thin-film. As is clearly seen from the fast reaction in the uncoated parts of the electrode, a possible kinetic control by the Butler–Volmer interface can be significant only on the way shorter time scale of a few seconds. Thus, the origin of the here-determined barrier coefficient has to be unambiguously attributed to the interface between the rock-salt and the spinel phases, at which the majority of the Li atoms are forced to change their interstitial position from 16c to 8a. Such barrier coefficient originating from the phase boundary has not been evaluated in any battery electrode previously, although Berkemeier et al.^[20] did report the barrier coefficient for lithium migration for the Butler–Volmer interface in the case of lithium cobalt oxide.

The possible microscopic origin of the kinetic barrier to boundary migration needs further consideration. In the classical case of intermetallic growth via substitutional interdiffusion, and even in the case of interstitial compounds such as the growth of silicides^[10–12] and hydrides,^[13,14] the existence of a kinetic barrier has been justified by the hindered migration of atoms through the phase boundary. Given the fast growth of the spinel phase beyond the interface, this is probably not the case here, (cf. concentration profile in Figure 4d). Furthermore, the barrier coefficient is usually seen as a generic property of the interface while the diffusion coefficient is a generic property of the volume, both certainly not depending on the diffusion geometry. Therefore, the here observed dependence of the kinetic transition on the sample geometry is an absolutely striking result that provokes an attempt of a plausible explanation from us.

A detailed kinetic modeling of the observed effect is beyond the scope of this experimental study, but at least one possible

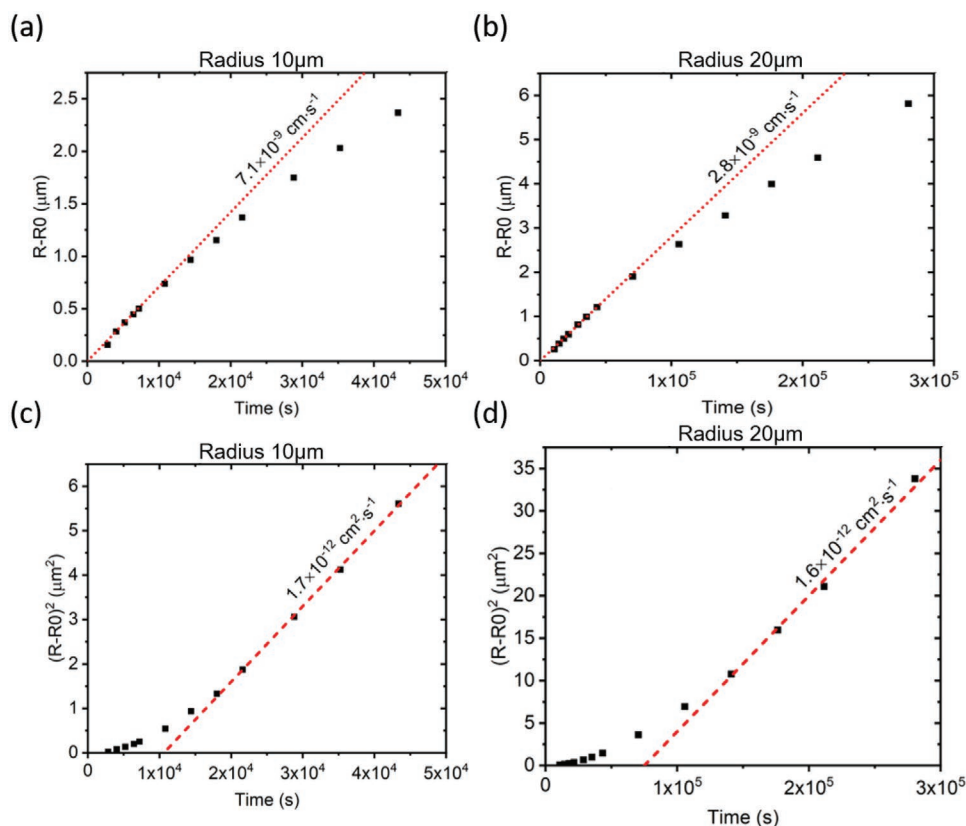


Figure 7. Growth of Li-rich phase in the circular geometry with radius a) 10 μm and b) 20 μm . c) and d) show the corresponding plots of the square of width versus time, respectively.

interpretation should be outlined here. We will restrict this consideration to the particular transparent case of a (001) interface orientation, which can only partly reflect the real situation of a nano-crystalline material, in which the phase boundary has to cross many grains of different orientations. However, according to other reports, the (001) orientation plays a predominant role so that the phase boundary may reveal extended facets of the (001) orientation.^[45,46] Even for any other interface orientation, the Li atoms sense a similar situation of frustration in the occupation of 8a and 16c sites, the general features might be independent of the particular interface orientation. In the exemplary (see **Figure 8a** showing only lithium atoms), the Li sites are stacked in the diffusion direction alternating between planes of two 8a-sites (per cubic unit cell with 32 atoms), each having two possibilities for the forward jumps to neighbored 16c-sites, and planes of four 16c-sites, each having only a single jump possibility to an 8a site in the forward direction. A lithium atom in the rock salt phase is likely to be occupying a 16c site, and if it were to jump forward into the spinel phase, it needs to move via an empty 8a site (as shown by the dotted arrow at the Li-rich side).^[26,44,45,47] The subsequent jump will occur into the empty 16c in the spinel phase, in which most of the 8a sites are filled. However, due to coulombic repulsion between 8a and 16c sites,^[16,22] soon after the Li-ion has occupied the 16c site, it will propagate further, resulting in the outward flux into the volume of the spinel phase with a much higher diffusion coefficient. Only in

statistically rare cases, simultaneous jumps by further atoms from 8a (corner atoms at the phase boundary, highlighted by the polyhedral with dark yellow edges in **Figure 8a**) into neighbored 16c sites may enable to form a nucleus of a next lattice plane of the rock salt phase and so will result in the net movement of the phase boundary.

In consequence, at least two planes must appear at the interface where the Li occupancy is disturbed with respect to the adjacent phase volume. This concentration disturbance at the interface has been postulated using DFT calculations.^[7] So, we may draw the energy landscape of the Li sites close to the interface as schematically sketched in **Figure 8b** (the proposed energy landscape is rationalized by the calculation performed by Ziebarth et al.^[44]). Before the interface, the (Gibbs) energy of an 8a-site is high while that of a 16c-site is low, beyond the interface just the opposite holds. But at the two interface planes, the site energies of 8a and 16c approach to an intermediate level because of the disturbed next-neighborhood. For convenience, we have numbered the planes fixing the origin to the 8a plane in the interface. A migration of the interface to the right-hand side requires nucleation of a new rock-salt double-layer, meaning, at least a cooperative shift of Li-ions from the 8a-sites on plane #0 to 16c-sites of plane #1. Such nucleation needs a minimum driving force by Li supersaturation at the interface with respect to the equilibrium level in the spinel phase. Thus, the Li concentration on the two interfacial planes (#0, #1) becomes decisive for further migration of the interface. In a steady-state

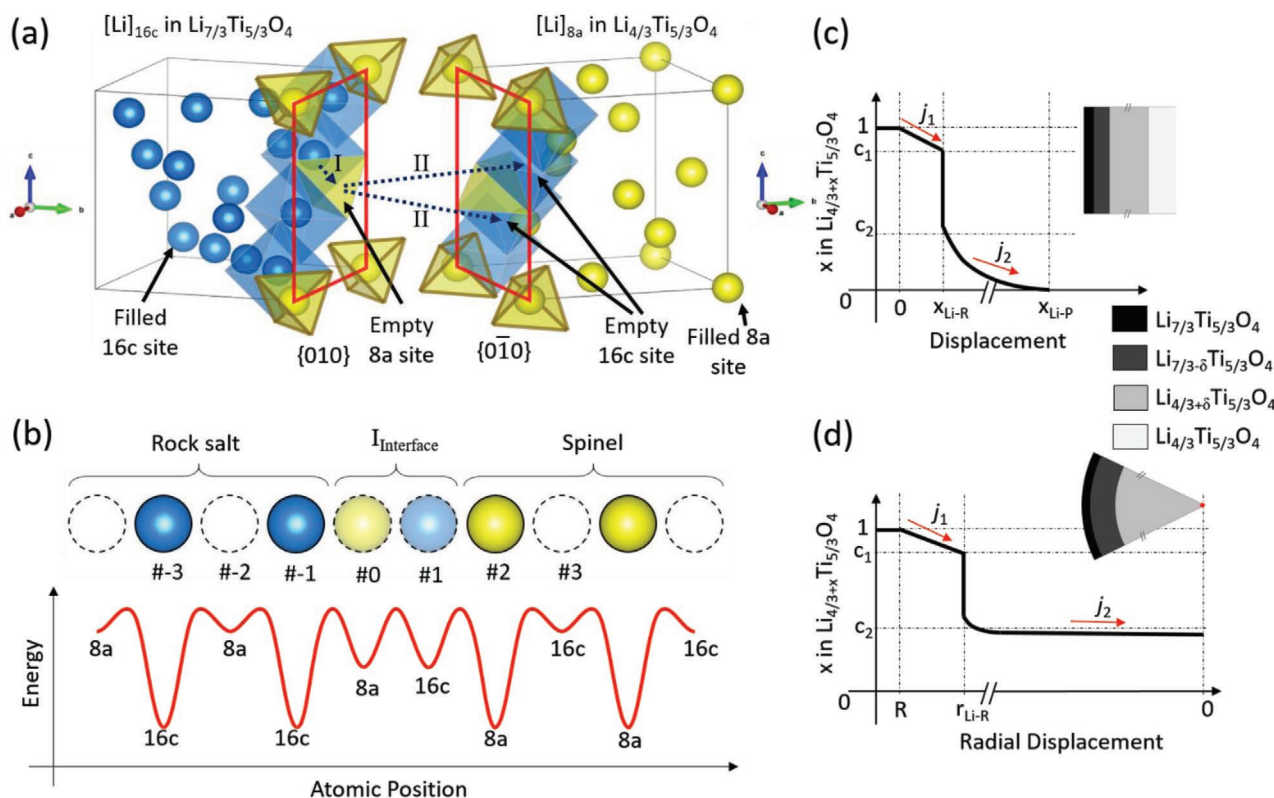


Figure 8. a) Position of Li-atoms at 16c sites (Blue) and 8a sites (Yellow) in rock salt and spinel phases, and the dotted line shows migration of a lithium atom as shown by dashed arrow, at the phase boundary (highlighted by red edges). b) Distribution of Li atoms in an exemplary diffusion direction, when viewed from $\langle 001 \rangle$ direction. The White (dashed edges), Blue, and Yellow circles represent the empty sites, the filled 16c sites, and 8a site. The light-blue and yellow circles (dashed edges) represent the partially filled 16c and 8a sites at the phase boundary region. The probable energy distribution at 16c and 8a sites when moving from rock salt (on left) to spinel phase on the right. Illustrative concentration profiles in the diffusion direction for: c) Semi-infinite diffusion geometry; and d) A spherical (or circular) particle of radius R , undergoing the phase transformation via radially inward flux, when the spinel phase has completely saturated the particle.

situation, this concentration is controlled by the Li fluxes in the vicinity to the interface, formally expressed as:

$$j_{-1 \rightarrow 0} = v_{c \rightarrow a}^R c_c^R (1 - c_a^I) \quad (3a)$$

$$j_{0 \rightarrow 1} = 2v_{a \rightarrow c}^I c_a^I (1 - c_c^I); j_{1 \rightarrow 0} = v_{c \rightarrow a}^I c_c^I (1 - c_a^I) \quad (3b,c)$$

$$j_{1 \rightarrow 2} = v_{c \rightarrow a}^I c_c^I (1 - c_a^S); j_{2 \rightarrow 1} = 2v_{a \rightarrow c}^S c_a^S (1 - c_c^I) \quad (3d,e)$$

$$j_{2 \rightarrow 3} = 2v_{a \rightarrow c}^S c_a^S (1 - c_c^S) \quad (3f)$$

In these equations, j , v and c represent the directed fluxes between the indexed planes, the jump frequencies (affected by the site energy via Boltzmann activation factors), and the Li concentration on the indexed plane, respectively; the super and subscript indexes have their natural meaning in the present context (I: interface, S, R: the two phases, that is, spinel and rock-salt, a: 8a-site, c: 16c-site). In the non-equilibrium situation of linear growth, the backward flux $j_{0 \rightarrow 1}$ can be neglected relative to the corresponding forward flux $j_{-1 \rightarrow 0}$, since the applied cell voltage forces the concentration of Li in the rock salt (c_c^R) much higher than equilibrium, that is, tending toward 1. Initially, the

concentration gradient in the spinel phase beyond the interface is large and so is the drain flux $j_{2 \rightarrow 3}$, therefore c_a^S in Equation (3e) is depressed (as lithium is driven away by the high $j_{2 \rightarrow 3}$ from position #2) and therefore the backward flux $j_{2 \rightarrow 1}$ becomes negligible. Consequently, the Li supersaturation at the interface is low and constant, solely defined by the balance between the forward fluxes $j_{-1 \rightarrow 0}$ and $j_{1 \rightarrow 2}$. In consequence, the nucleation of the new rock-salt structure and thus the migration of the interface appears with a rather slow but constant rate, that is, interface migration appears proportionally to time. In the course of further intercalation, however, the concentration gradient in the spinel relaxes and so does the forward flux $j_{2 \rightarrow 3}$ (Equation (3f)). Consequently, the back flux $j_{2 \rightarrow 1}$ increases. As soon as it becomes comparable to the corresponding forward flux $j_{1 \rightarrow 2}$, the Li concentration at the interface increases significantly, and with this the nucleation rate of new rock salt planes, too. Eventually, the nucleation rate becomes sufficiently high that the diffusion transport across the formed rock salt layer starts limiting the further phase growth which then leads to a parabolic time dependence.

In this scenario, we see that the concentration gradient in the spinel phase, although located ahead of the interface (phase boundary), makes a decisive impact owing to the competition for Li that either increases the supersaturation at the interface or drains into the spinel. Since the Li diffusion width in the

spinel is considerably larger than in the rock salt, the reduction of diffusion space in the studied finite-sized circular structures, leads to a much earlier saturation of the Li content in the spinel phase and therefore depresses the further Li drain (see the illustrative concentration profiles in Figure 8c,d for the semi-infinite and finite circular geometry). In final consequence, it is no more the critical thickness of the rock salt phase, but the diffusion depth within the spinel which controls the transition into the parabolic regime, exactly as observed in the experiment. For the practical realization of a battery, the anode particles must be chosen small enough so that diffusion width in the Li-poor phase gets early limited by the particle size and so the slow linear regime of phase growth is depressed.

As mentioned before, in a recent theoretical study, Ganapathy et al.^[45] using first-principle calculations, addressed already the migration across the phase boundary and its movement during the phase transformation. Based on their calculation, they postulate that the interface behaves almost like a liquid, meaning extremely high mobility, which stands in striking contrast to the here presented experiments. However, it should be noted that the molecular dynamics study could only consider a very short time period of 200 ps and a rather small volume of 4 unit cells in a periodic boundary conditions, which does not allow studying nucleation processes. Even out of the 200 ps, the first half is needed to establish a kind of equilibrium from the starting configuration. Indeed, a significant mean square displacement of the Li ions has been simulated in this transient period. But later, the calculated average displacement saturates, so that real equilibrium diffusion is hardly demonstrated in simulation. According to our experimental observation, even when extrapolating to the higher temperature of the simulation (600 K), the interface would move way less than a single atomic distance, $\approx 10^{-13}$ m, within a period of 200 ps. A similar discrepancy is noticed when comparing the simulated mean square displacements with the experimentally measured diffusion coefficients. Obviously, significantly different kinetic processes are considered in the ab-initio calculation and our experiments.

In view of the schematic potential landscape in Figure 8b, the simulations have probably revealed the high jumping rate in the frustration zone along the interface (planes #0,1), where the Li ions have relative high site energies on 8a and 16c sides as well and thus could jump frequently. But fast jumps, back and forth, along the interface do neither support the macroscopic migration of the interface nor the long range transport of the Li ions. (Strictly speaking, diffusion needs to be studied in the limit of infinite time to clarify all correlation effects between atomic jumps.)

4. Conclusion

- A new methodology to study lithium transport in thin-film battery electrodes has been reported. It exploits the electrochromic activity of lithium titanate and enables quantitative evaluation in terms of averaged transport coefficients and activation energy. The optical contrast in circular patterns provides convincing evidence for a two-phase core-shell lithiation reaction.

- The diffusion coefficient for lithium in the rock salt phase $\text{Li}_{7/3-\delta}\text{Ti}_{5/3}\text{O}_4$ at 22 °C was determined to be $2.65 \times 10^{-12} \text{ cm}^2 \cdot \text{s}^{-1}$ with an activation energy of 0.76 eV. The diffusion of lithium in the spinel phase $\text{Li}_{4/3+\delta}\text{Ti}_{5/3}\text{O}_4$ is about seven times faster with an activation energy of 0.70 eV.
- A linear-to-parabolic transition in the phase growth of the rock salt phase demonstrates a kinetic barrier against migration of the phase boundary. Provided unrestricted diffusion in the spinel phase, the respective barrier coefficient amounts to $3.84 \times 10^{-9} \text{ cm} \cdot \text{s}^{-1}$ at 22 °C with an activation energy of 0.86 eV. The barrier at the interface significantly slows down the growth of the rock salt phase up to a phase-width of $\approx 4 \mu\text{m}$. However, if diffusion flux into the spinel phase is blocked, the migration barrier against phase growth is diminished.
- A conceptual interpretation has been proposed that the migration of the phase boundary is controlled by continuous nucleation of new interstitial planes of the rock salt phase. The rate of this nucleation depends on the Li supersaturation at the interface and so can be controlled by the diffusion flux into the spinel phase. As a practical consequence, the overall kinetics of intercalation in nano- or micro-particles is effectively controlled by the achieved diffusion width in the spinel phase rather than by the slow diffusion in the rock salt phase or a kinetic transport barrier at the interface.

Extracting from the above drawn conclusions, the study uncovers a previously overlooked significance of the reduction of the electrode particle size on the performance of the LTO electrode. With the new evidence, we can clearly say that the reduction of particle size will enable quick saturation of the electrodes with the spinel phase due to much faster diffusivity of lithium in this phase. This saturation will effectively suppress the drain of Li-flux into the spinel phase, thereby enabling quicker nucleation and growth of the rock salt phase, hence, maximizing the capacity obtained during fast charging performance in practical electrodes.

5. Experimental Section

Thin-Film Preparation: Radio-frequency ion-beam sputtering (Rau&Roth, 4 cm ϕ) was used for the preparation of thin films. Polished oxidized silicon wafers were used as substrates. A thin platinum metallization (180 nm), acting as a current collector, was first sputtered onto the wafer followed by a layer of the LTO electrode (260 nm). The LTO layer was deposited using argon/oxygen plasma in the deposition chamber (9:1 ratio of Ar:O₂). A cold-pressed powder (EXM 1037-Li₄Ti₅O₁₂, Südchemie) was used as the target for the LTO deposition.^[48] The platinum deposition was carried out without oxygen (i.e., under pure argon). A schematic of the sputter chamber and more details on the deposition conditions are given in refs. ^[9,49] After the deposition, the layers were annealed at 550 °C in vacuum for 2 h. Only the annealed samples showed the proper reversible Li intercalation and were used throughout the study.

Electrochromic Imaging: This imaging technique was developed to study the diffusion of lithium and the resulting phase transformation in thin-film electrodes. Figure 1a,b shows the schematics of the sample and the setup used, respectively. The sample had a lithium blocking area coated with SU-8, structured with the help of a lithography process, described in the subsequent section. The electrochemical cell, shown in Figure 1b, consisted of a three-electrode setup controlled by a Gamry Interface 1000 potentiostat. Two lithium foils acted as reference and

counter electrodes. Hence, all the potentials mentioned in the text were stated with respect to lithium. In this study, the use of a three-electrode setup enabled independent measurement of the voltage of the working electrode versus a third lithium electrode which did not participate in the reaction (i.e., zero current flowed through this electrode). This made it possible to maintain a stable voltage or a constant electrochemical potential in the bulk of LTO (except from surface overpotentials).

A platinum metallization provided the electrical contact to the LTO electrode which was acting as the working electrode. 1 M LiClO₄ in ethylene carbonate and dimethyl carbonate (1:1 ratio by mass) was used as the liquid electrolyte. The electrochemical cell was assembled in an argon-filled glovebox and was subsequently sealed. The cell had flat faces and was made of optical grade glass (Hellma Analytics 700.016-OG). It was held by a custom-build holder (made from Polyether ether ketone, PEEK) which had two Peltier elements (from Adaptive, manufacture part number ET-031-10-13-RS) placed on two opposite sides of the cell. The Peltier elements were used for heating the cell. Additionally, a K-type thermocouple was inserted in the electrochemical cell to monitor the temperature throughout the measurement. A Mitutoyo microscope unit, with a 10× objective lens (Mitutoyo Plan Apo Infinity corrected long WD objective), was fixed horizontally to focus on the interface of the bare LTO and SU-8 coated LTO. A color filter was placed before a camera (Thorlabs DCC1645C) allowing only light with a wavelength greater than 590 nm to pass. The choice of the filter was based on the previous study reporting that Li_{7/3}Ti_{5/3}O₄ phase shows the most dominant optical absorption in the red wavelength.^[9] To study the diffusion of lithium underneath the barrier layer, a constant voltage of 1 V was applied at time $t = 0$ s and was maintained throughout the experiment; simultaneously the camera recorded images at particular time intervals. The small difference in grey level due to the SU-8 layer, variation in the lamp intensity (during the course of the experiment), and the change in absorption of light by the electrolyte were corrected by a calibrating the intensity obtained by each gray scale image from a section from the uncoated LTO and a section far away underneath the SU-8 (i.e., not participating in the reaction). This was technically achieved by a multiplication factor (only for intensity) and an offset to match the intensity of the fully intercalated Li_{7/3}Ti_{5/3}O₄ phase, in the uncovered SU-8 and the fully de-lithiated LTO phase underneath the SU-8. Furthermore, the drift in the measurement was corrected by aligning the interface (between the bare LTO and SU-8 coated LTO) for all the analyzed frames. Lithiation was studied at three temperatures, that is, 22, 45, and 55 °C. Regarding the choice of the temperature, the upper limit was restricted by the electrolyte and the lower (22 °C, room temperature) by the experimental time window (2 weeks). The possibility to measure the kinetics at higher temperatures were tested, but the solvent of the electrolyte degraded quite fast at temperatures above 60 °C as has also been mentioned in a paper by Cao et al.^[50] This results in the severe loss of the optical resolution and hence the results were not appropriate for accurate analysis. Moreover, the higher the temperature, the smaller will be the linear regime, as is also clear in Figure 5. Hence, evaluation of temperatures higher than 60 °C would probably result in only diffusion controlled parabolic growth of the Li-rich phase.

Lithography: After the required annealing of the active material, electron (e-) beam lithography was used to coat an area with a lithium blocking layer. Kayaku Advanced Materials SU-8 2000.5 photo/e-beam resist (a negative photoresist) was used as a blocking layer, due to its inability to dissolve in organic solvents (present in the battery electrolyte) and because of its crosslinking nature (upon exposure to e-beam) which probably helped in effectively blocking the lithium-ion. The schematics of the samples are given in Figure 1a.

The layer of SU-8 2000.5 was spin-coated at 1000 rpm for 30 s. Followed by a prebake at 95 °C for 2 min. Subsequently, the sample was transferred into the SEM (FEI Scios Dual-beam microscope). A selected area (600 × 550 μm²) was exposed with a dose of 1.5 μC cm⁻² at 30 kV and using a current of 3.1 pA with a pitch of ≈155 nm. Subsequently, the sample was post-baked at 95 °C for 4 min followed by developing it with propylene glycol monomethyl ether acetate (or PGMEA) (Sigma-Aldrich, CAS number: 108-65-6). The sample was rinsed with iso-propanol and

dried in air. Finally, a hard-bake was executed at 150 °C for 30 min in air to further crosslink the SU-8.

To study the effect of electrode geometry on the growth kinetics, circular patterns were coated with diameters of 40, 20, 10, and 5 μm. The lithography used the same methodology, except that the pitch between each illuminated spot was 13 nm.

The quality/morphology of the lithography has been verified by an FEI Quanta SEM. The microstructure of the layers, with and without the SU-8, has been determined by TEM using a Philips CM200-FEG instrument. For this, electron transparent foils were prepared by lifting out a lamella using an FEI Scios dual-beam microscope (FIB-SEM).^[51]

Supporting Information

Supporting Information is available from the Wiley Online Library or from the author.

Acknowledgements

Joint support by the Deutsche Forschungsgemeinschaft (DFG, INST 41/982-1) and the Baden-Württemberg Foundation in the acquisition of the dual-beam microscope is gratefully acknowledged.

Open access funding enabled and organized by Projekt DEAL.

Conflict of Interest

The authors declare no conflict of interest.

Data Availability Statement

Research data are not shared.

Keywords

diffusion, electrochromic imaging, Li₄Ti₅O₁₂, linear to parabolic transitions, phase transformation

Received: May 18, 2021

Revised: July 29, 2021

Published online: August 21, 2021

- [1] X. Sun, P. V. Radovanovic, B. Cui, *New J. Chem.* **2015**, 39, 38.
- [2] T. Yuan, Z. Tan, C. Ma, J. Yang, Z.-F. Ma, S. Zheng, *Adv. Energy Mater.* **2017**, 7, 1601625.
- [3] D. W. Murphy, R. J. Cava, S. M. Zahurak, A. Santoro, *Solid State Ionics* **1983**, 9–10, 413.
- [4] T. Ohzuku, A. Ueda, N. Yamamoto, *J. Electrochem. Soc.* **1995**, 142, 1431.
- [5] M. Wagemaker, D. R. Simon, E. M. Kelder, J. Schoonman, C. Ringpfeil, U. Haake, D. Lützenkirchen-Hecht, R. Frahm, F. M. Mulder, *Adv. Mater.* **2006**, 18, 3169.
- [6] M. Wagemaker, E. R. H. van Eck, A. P. M. Kentgens, F. M. Mulder, *J. Phys. Chem. B* **2009**, 113, 224.
- [7] X. Lu, L. Zhao, X. He, R. Xiao, L. Gu, Y.-S. Hu, H. Li, Z. Wang, X. Duan, L. Chen, J. Maier, Y. Ikuhara, *Adv. Mater.* **2012**, 24, 3233.
- [8] C. Y. Ouyang, Z. Y. Zhong, M. S. Lei, *Electrochem. Commun.* **2007**, 9, 1107.

- [9] Y. Joshi, A. Saksena, E. Hadjixenophontos, J. M. Schneider, G. Schmitz, *ACS Appl. Mater. Interfaces* **2020**, 12, 10616.
- [10] B. Parditka, H. Zaka, G. Erdélyi, G. A. Langer, M. Ibrahim, G. Schmitz, Z. Balogh-Michels, Z. Erdélyi, *Scr. Mater.* **2018**, 149, 36.
- [11] F. Nemouchi, D. Mangelinck, C. Bergman, P. Gas, U. Smith, *Appl. Phys. Lett.* **2005**, 86, 041903.
- [12] B. E. Deal, A. S. Grove, *J. Appl. Phys.* **1965**, 36, 3770.
- [13] E. Hadjixenophontos, K. Zhang, A. Weigel, P. Stender, G. Schmitz, *Int. J. Hydrogen Energy* **2019**, 44, 27862.
- [14] E. Hadjixenophontos, L. Michalek, M. Roussel, M. Hirscher, G. Schmitz, *Appl. Surf. Sci.* **2018**, 441, 324.
- [15] R. Ma, L. Shao, K. Wu, M. Shui, D. Wang, J. Pan, N. Long, Y. Ren, J. Shu, *ACS Appl. Mater. Interfaces* **2013**, 5, 8615.
- [16] W. Zhang, D. H. Seo, T. Chen, L. Wu, M. Topsakal, Y. Zhu, D. Lu, G. Ceder, F. Wang, *Science* **2020**, 367, 1030.
- [17] M. Muñoz-Castro, F. Berkemeier, G. Schmitz, A. Buchheit, H.-D. Wiemhöfer, *J. Appl. Phys.* **2016**, 120, 135106.
- [18] Y. Joshi, E. Hadjixenophontos, S. Nowak, R. Lawitzki, P. K. Ghosh, G. Schmitz, *Adv. Opt. Mater.* **2018**, 6, 1701362.
- [19] M. Rubin, K. Von Rottkay, S.-J. J. Wen, N. Özer, J. Slack, *Sol. Energy Mater. Sol. Cells* **1998**, 54, 49.
- [20] F. Berkemeier, T. Stockhoff, T. Gallasch, G. Schmitz, *Acta Mater.* **2014**, 80, 132.
- [21] A. J. Merryweather, C. Schnedermann, Q. Jacquet, C. P. Grey, A. Rao, *Nature* **2021**, 594, 522.
- [22] W. Schmidt, P. Bottke, M. Sternad, P. Gollob, V. Hennige, M. Wilkening, *Chem. Mater.* **2015**, 27, 1740.
- [23] H. Hain, M. Scheuermann, R. Heinzmann, L. Wünsche, H. Hahn, S. Indris, *Solid State Nucl. Magn. Reson.* **2012**, 42, 9.
- [24] M. Vijayakumar, S. Kerisit, K. M. Rosso, S. D. Burton, J. A. Sears, Z. Yang, G. L. Graff, J. Liu, J. Hu, *J. Power Sources* **2011**, 196, 2211.
- [25] M. Wilkening, W. Iwaniak, J. Heine, V. Epp, A. Kleinert, M. Behrens, G. Nussli, W. Bensch, P. Heitjans, *Phys. Chem. Chem. Phys.* **2007**, 9, 6199.
- [26] Y. C. Chen, C. Y. Ouyang, L. J. Song, Z. L. Sun, *Electrochim. Acta* **2011**, 56, 6084.
- [27] C. Wang, S. Wang, Y.-B. He, L. Tang, C. Han, C. Yang, M. Wagemaker, B. Li, Q.-H. Yang, J.-K. Kim, F. Kang, *Chem. Mater.* **2015**, 27, 5647.
- [28] L. G. Harrison, *Trans. Faraday Soc.* **1961**, 57, 1191.
- [29] S.-L. Chou, J.-Z. Wang, H.-K. Liu, S.-X. Dou, *J. Phys. Chem. C* **2011**, 115, 16220.
- [30] J. Ma, Y. Wei, L. Gan, C. Wang, H. Xia, W. Lv, J. Li, B. Li, Q.-H. Yang, F. Kang, Y.-B. He, *J. Mater. Chem. A* **2019**, 7, 1168.
- [31] J. Wang, H. Zhao, Z. Li, Y. Wen, Q. Xia, Y. Zhang, G. Yushin, *Adv. Mater. Interfaces* **2016**, 3, 1600003.
- [32] Z. Balogh-Michels, G. Schmitz, *Physical Metallurgy: Fifth Edition*, Elsevier, New York **2014**, pp. 387–559.
- [33] D. A. Porter, K. E. Easterling, M. Y. Sherif, *Phase Transformations in Metals and Alloys*, Third Edition, CRC Press, Boca Raton, FL **2009**.
- [34] G. V. Kidson, *J. Nucl. Mater.* **1961**, 3, 21.
- [35] J. J. Tomán, G. Schmitz, Z. Erdélyi, *Comput. Mater. Sci.* **2017**, 138, 183.
- [36] U. Gösele, K. N. Tu, *J. Appl. Phys.* **1982**, 53, 3252.
- [37] C. Wagner, *Acta Metall.* **1969**, 17, 99.
- [38] C. Matano, *Jpn. J. Phys.* **1933**, 8, 109.
- [39] M. Okugawa, H. Numakura, *Metall. Mater. Trans. A* **2015**, 46, 3813.
- [40] F. Ernst, A. Avishai, H. Kahn, X. Gu, G. M. Michal, A. H. Heuer, *Metall. Mater. Trans. A* **2009**, 40A, 1768.
- [41] J. Crank, E. P. J. Crank, *The Mathematics of Diffusion*, Clarendon Press, Oxford **1979**.
- [42] M. Wilkening, R. Amade, W. Iwaniak, P. Heitjans, *Phys. Chem. Chem. Phys.* **2007**, 9, 1239.
- [43] J. Haetge, P. Hartmann, K. Brezesinski, J. Janek, T. Brezesinski, *Chem. Mater.* **2011**, 23, 4384.
- [44] B. Ziebarth, M. Klinsmann, T. Eckl, C. Elsässer, *Phys. Rev. B: Condens. Matter Mater. Phys.* **2014**, 89, 174301.
- [45] S. Ganapathy, A. Vasileiadis, J. R. Heringa, M. Wagemaker, *Adv. Energy Mater.* **2017**, 7, 1601781.
- [46] M. Kitta, T. Akita, S. Tanaka, M. Kohyama, *J. Power Sources* **2014**, 257, 120.
- [47] W. Schmidt, M. Wilkening, *J. Phys. Chem. C* **2016**, 120, 11372.
- [48] F. Wunde, F. Berkemeier, G. Schmitz, *J. Power Sources* **2012**, 215, 109.
- [49] S. Nowak, F. Berkemeier, G. Schmitz, *J. Power Sources* **2015**, 275, 144.
- [50] X. Cao, X. He, J. Wang, H. Liu, S. Röser, B. R. Rad, M. Evertz, B. Streipert, J. Li, R. Wagner, M. Winter, I. Cekic-Laskovic, *ACS Appl. Mater. Interfaces* **2016**, 8, 25971.
- [51] L. A. Giannuzzi, J. L. Drown, S. R. Brown, R. B. Irwin, F. A. Stevie, *Microsc. Res. Tech.* **1998**, 41, 285.